Combined effect of gallium and carbon on the structure and magnetic properties of nanocrystalline $SmFe_9$



2006 J. Phys.: Condens. Matter 18 3845

(http://iopscience.iop.org/0953-8984/18/15/027)

INSTITUTE OF PHYSICS PUBLISHING JOURNAL OF PHYSICS: CONDENSED MATTER

J. Phys.: Condens. Matter **18** (2006) 3845–3859 doi:10.1088/0953-8984/18/15/027

# Combined effect of gallium and carbon on the structure and magnetic properties of nanocrystalline $SmFe_9$

**L Bessais**[1], **E Dorolti and C Djéga-Mariadassou**

LCMTR, UPR209, CNRS, 2/8 rue Henri Dunant, BP 28, F-94320 Thiais, France

E-mail: bessais@glvt-cnrs.fr

Received 15 December 2005, in final form 28 February 2006
Published 30 March 2006
Online at stacks.iop.org/JPhysCM/18/3845

**Abstract**

$SmFe_{9-y}Ga_xC$ carbides ($0 \leqslant x \leqslant 1$) were prepared by a two-step method of powder high-energy milling with annealing between 873 and 1200 K and a subsequent carbonation with heavy hydrocarbon at 693 K. The x-ray diffraction analysis with the Rietveld technique indicates an anisotropic volume expansion under carbonation slackened by the gallium substitution. The average saturation magnetic moment per Fe atom, measured with an applied field up to 200 kOe, increases slightly to 2.00 $\mu$B with Ga content. The Curie temperature, always 15 K above that of the homologous 2/17 carbides, is reduced by a dilution effect with Ga substitution and a concomitant increase of the negative Fe–Fe interactions. The Mössbauer spectra have been analysed on the basis of the binomial law related to the different Fe environments. The hyperfine parameter assignment to each individual crystallographic site was performed according to the correlation between isomer shift and Wigner–Seitz cell volumes calculated with a specific code in the $P1$ space group allowing the splitting of the partially occupied atomic positions. The role of the C insertion is shown, on the one hand, by the increase of isomer shift due to the volume expansion with an enhancement of the charge transfer from the rare-earth atoms and, on the other hand, by the hyperfine field increase, pointing out the predominance of the negative core electron polarization term. The coercive field of 27 kOe, combined with a Curie temperature of 680 K, makes the alloy $SmFe_{8.75}Ga_{0.25}C$ promising for further applications in the field of high-performance permanent magnets.

(Some figures in this article are in colour only in the electronic version)

## 1. Introduction

The prospect of advanced permanent magnet materials remains focused on the mastery of coercivity resulting from a combined control of high magnetocrystalline anisotropy and

[1] Author to whom any correspondence should be addressed.

microstructure. The most fertile route is the exploration of rare earth–iron based alloys structured on a magnetic length scale covering the nanoscale range.

$Sm_2Fe_{17}$ exhibits a low Curie temperature and a planar anisotropy at room temperature which restricts its possible applications as a permanent magnet. In order to overcome such hindrances, the substitution of s–p elements for Fe (Si, Al, Ga) or the introduction of interstitial atoms such as C or N is required. Moreover, the optimization of the coercive force can be obtained by means of a controlled nanocrystallization for which the main paths are mechanical alloying and rapid quenching. High-energy milling with subsequent annealing appears indeed as the most convenient one, owing to the high homogeneity of the samples, and remains the most appropriate for highly volatile elements such as samarium. Nevertheless, these techniques favour the formation of metastable phases. We had previously demonstrated by Rietveld analysis and Mössbauer spectroscopy [1] that the precursor of $Sm_2Fe_{17}$ is relevant to the hexagonal $P6/mmm$ space group described exclusively by the stoichiometry 1/9. Unlike nitrides obtained only by a solid–gas reaction, carbonation can be achieved by a solid–solid reaction. The study of out of equilibrium $Sm(Fe, Ga)_9$ carbides, never performed to date, is the aim of this present work.

In this paper, we focus attention on the intrinsic structural and magnetic characteristics of nanocrystalline carbides $SmFe_{9-y}Ga_yC$ up to $y = 1$. For the first time, high-field magnetization measurements have been performed; the accurate Mössbauer spectrum analysis based on the correlation between original Wigner–Seitz cell volume calculations and hyperfine parameters has been carried out. Our objective remains the evaluation of the ideally suitable alloy required for possible applications. Consequently, we have studied the coercivity as a function of the grain size of the non-carbonated host lattice. Moreover, the evolution of each mentioned parameter is presented. The study of these evolutions is presented together with those of a series $Sm_2Fe_{17-x}Ga_xC_2$ specifically prepared for comparison.

## 2. Experiment

The samples $SmFe_{9-y}Ga_y$ ($y = 0.25, 0.5, 0.75, 1$) were prepared by the high-energy ball milling technique with subsequent annealing of a mixture of pre-alloyed $Sm_2Fe_{17}$ and $Fe_3Ga$ (99.99%) with an excess of Sm powders in order to maintain a Sm overpressure on the sample.

The milling was performed in a Fritsch planetary mill for 5 h under high-purity argon atmosphere as explained previously [1–3], followed by crystallization treatments for 30 min at various temperatures between 873 and 1200 K.

The transfer of one C atom per unit formula 1/9 was monitored by reacting the $SmFe_{9-y}Ga_y$ alloys ground to less than 32 $\mu$m powder size with a balanced weight of $C_{14}H_{10}$ powder at 693 K for 24 h. The overpressure of hydrogen was absorbed by Mg chips inside the reacting tube.

X-ray diffraction was performed with Cu K$\alpha$ radiation on a Bruker diffractometer with an internal Si standard to insure a unit cell parameter accuracy of $\pm 1 \times 10^{-3}$ Å. The intensities were measured from $2\theta = 20°$–$110°$ with a step size of 0.04° and counting rate of 22 s per scanning step. The data treatment was carried out by a Rietveld refinement of the experimental and theoretical intensities with the FULLPROF computer code, in the assumption of a Thompson–Cox–Hastings line profile [1–4].

Isotropic Lorentzian and Gaussian contribution of size and micro-strains were taken into account. The full width at half maximum of the Gaussian $H_G$ and Lorentzian $H_L$ component of the profile function is given by

$$H_G^2 = u \tan^2 \theta + v \tan \theta + w$$

$$H_L = \zeta \tan\theta + \frac{\xi}{\cos\theta}$$

$\xi$ represents the volume averaged diameter of crystallites in all directions and provides the autocoherent diffraction domain size value ($D$). The $u$ parameter leads to an estimate of the isotropic broadening due to strain effects.

The various structural parameters, $X$, $Z$ atomic position, Debye Waller factor and occupancy parameter $s$, cell parameter and the $u$ and $\xi$ profile parameter, were least square fitted.

The 'goodness-of-fit' indicators are calculated as follows:

$$R_B = \frac{\sum_K |I_K(o) - I_K(c)|}{\sum_K I_K(o)}$$

$I_K(o)$ is the observed Bragg intensity and $I_K(c)$ is the calculated one.

High-resolution transmission electron microscopy (HRTEM) in bright-field mode and elemental analysis were carried out on a JEOL 2010 high-resolution transmission electron microscope operating at 200 kV, equipped with an energy dispersive x-ray (EDX) detector. The sample powders were imbedded in epoxy and microtomed to a thickness around 70 nm prior to imaging. Magnification from 40 000 to 800 000 was used. Inter-fringe measurements were performed and confirmed by Fourier transform images obtained with local software on digitized negatives. Systematic EDX measurements were carried out for each experiment with a spot size of 10 nm in order to *in situ* verify the nature of observed species.

Curie temperatures were measured within an accuracy of $\pm 1°$ with a differential sample magnetometer MANICS in a field of 1000 Oe with samples under vacuum. Isothermal magnetization ($M$) versus field ($H$) curves were recorded in Grenoble High Magnetic Field Laboratory. The extraction technique was used to measure the magnetization in a continuous magnetic field up to 200 kOe produced by a Bitter type magnet. Magnetic measurements were carried out in the temperature range 4.2–300 K using an automatic system provided with a cryostat associated with a calorimeter. The experimental accuracy on $M$ is estimated to be $\pm 2\%$. A detailed description is given elsewhere [5]. Hysteresis curves ($M$–$H$) were measured at room temperature (RT) by PPMS9 (Quantum Design) with a maximum field of 90 kOe.

Mössbauer spectra at room temperature were collected with a conventional constant acceleration 512-channel spectrometer and a rhodium matrix cobalt-57 source, with $\alpha$-Fe line-width of 0.25 mm $s^{-1}$ and Fe sample concentration of 12 mg $cm^{-2}$. Isomer shift is relative to bcc-iron at 300 K. The estimated errors are $\pm 0.1$ T for hyperfine field $H_{HF}$, $\pm 0.005$ mm $s^{-1}$ for isomer shift $\delta$ and quadrupole split $2\epsilon$. The spectra were least square fitted in the assumption of Lorentzian lines according to the procedure discussed herein.

## 3. Results and discussion

### *3.1. Crystallographic analysis*

Figure 1 shows the XRD patterns of the carbonated samples $SmFe_{9-y}Ga_yC$ after carbonation at 693 K of $SmFe_{9-y}Ga_y$ powder annealed at 983 K. They all exhibit the hexagonal $P6/mmm$ phase and around ($\simeq$2 wt%) of $Sm_2O_3$ resulting, as expected, from the oxidation of the excess samarium in small grain size. A small amount of $\alpha$-Fe, around $\simeq$1 wt%, is observed due to the carbonation process, as no $\alpha$-Fe peak was detected in the sample before carbonation either on the x-ray diagram or on the Mössbauer spectra [2].

The Rietveld refinements (figure 2) have been performed on the basis of the structural description $Sm_{1-s}(Fe, Ga)_{5+2s}$ which results from the generalization of the model given

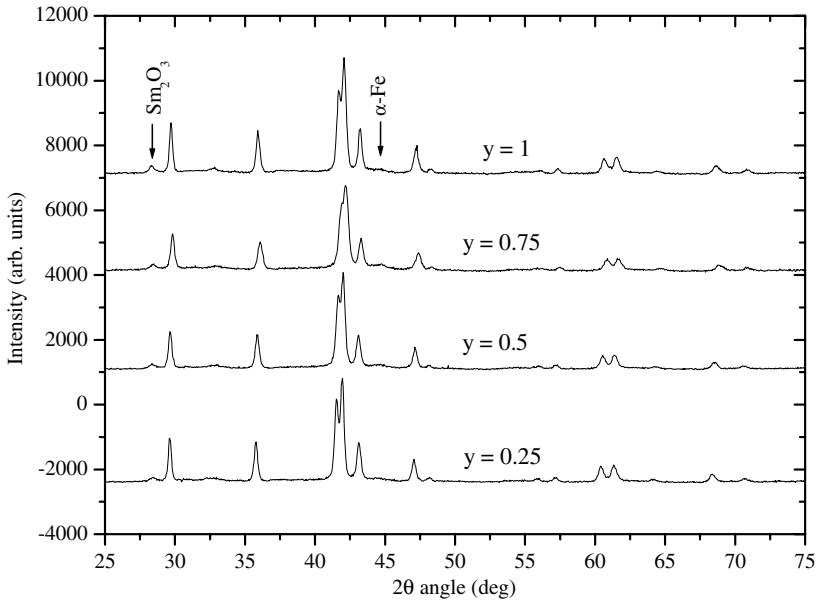


**Figure 1.** X-ray diagrams of $SmFe_{9-y}Ga_yC$ for $y = 0.25, 0.5, 0.75$, and 1.

previously [6] for small Co stoichiometry deviation of $SmCo_5$ alloys with a measured $s$ value equal to 0.03.

Let us recall that, *theoretically*, the $s$ parameter can cover all compositions from $RT_5$ to $RT_{12}$; R is a rare earth and T a transition metal. Between $s = 0$ ($RT_5$) and $s$ close to 0.33 (2/17), besides the R 1a(0, 0, 0), T 2e(0, 0, $z$), and T 3g(1/2, 0, 1/2) families, two close T families are implied to describe the composition evolution: 6l ($x$, $2x$, 0 ($x < 1/3$)) and 2c (1/3, 2/3, 0).

$s$ samariums in the 1a site (0, 0, 0) are substituted by $2s$ T atoms in the 2e site. There remain only $2(1 - 3s)$ T atoms in the general 2c position while $6s$ T atoms in the 6l position reflect the disturbance brought by the $s$ R vacancies. For $s \geqslant 0.33$ the 2c family does not exist any more. The T atoms occupy three non-equivalent sites. Three and two atoms are respectively in 3g and 6l sites. The 6l atoms maintain hexagons around the samarium vacancy along the $c$ axis and the T pairs (dumbbell) in the 2e site. In the carbides, C is located in the 3f position. This model is applied to the hexagonal $P6/mmm$ carbide precursor of $Sm_2Fe_{17}C_2$.

The minimum Rietveld agreement factor ($R_B$) is achieved for $s = 0.36$ with gallium located in the 3g site. It turns out that the precursor formula is $SmFe_{9-y}Ga_yC$. These results exclude the structure of $TbCu_7$ type ($s = 0.22$) generally invoked for the precursors of the 2/17 compounds [7]. The value $s = 0.36$ (1/9) for the precursor is close to the $s$ value of its 2/17 derivative ($s = 0.33$), which is not the case for the $TbCu_7$ structure ($s = 0.22$).

For the smallest Ga content up to $y = 0.75$, $\Delta a/a$ is equal to $+0.70\%$ per Ga atom with $c$ remaining constant. From $y = 0.75$ to 1, $a$ is constant while the $\Delta c/c$ ratio decrease is equal to $-0.84\%$/Ga atom. These evolutions imply a linear decrease of the unit cell volume $\Delta V/V$ of $-1.40\%$/Ga atom from $y = 0.25$ to 1.

The unit cell volume expansion under carbonation for a given Ga content is more pronounced for the low Ga contents than that of the equilibrium homologous 2/17 carbides. With $V'$ and $V$ respectively equal to the volumes of the carbonated cell and that of the non carbonated one [2], the ratio $(V' - V)/V$ varies from 4.78% to 2.72% for $y = 0.25$ and 1. These volume evolutions are only 3.8 and 2.72% for the $Sm_2(Fe, Ga)_{17}C_2$ compounds.

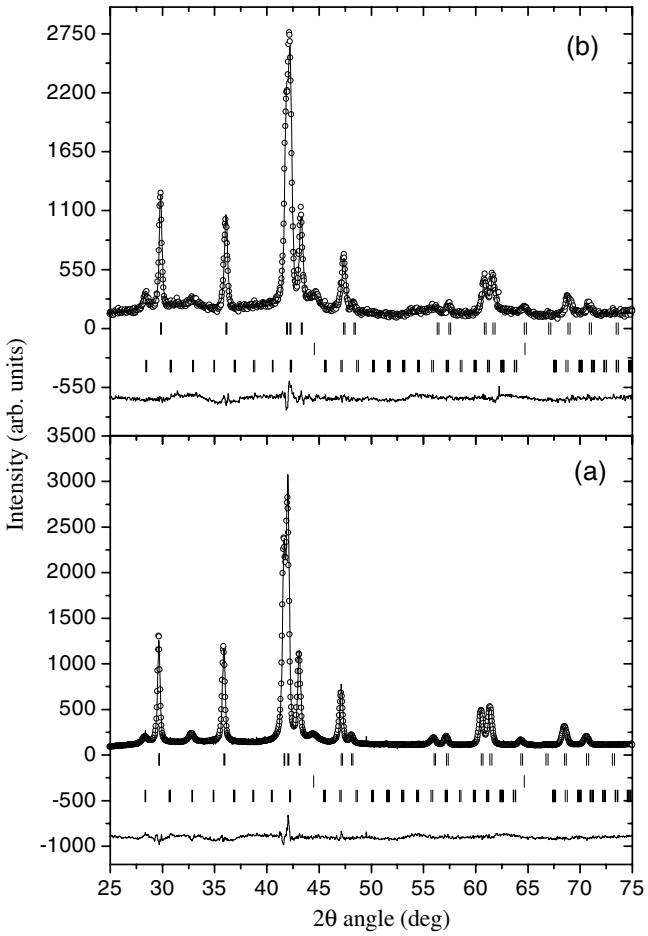


**Figure 2.** Rietveld analysis for (a) $SmFe_{8.75}Ga_{0.5}C$ and (b) $SmFe_{8.25}Ga_{0.75}C$. The sets of ticks refer, respectively, from top to bottom, to $P6/mmm$, $\alpha$-Fe, and $Sm_2O_3$.

The accurate structural parameters found, for the first time, for these out-of-equilibrium carbides will be used for the Wigner–Seitz cell (WSC) volume calculations necessary for a reliable Mössbauer spectrum analysis.

The nanocrystalline state is demonstrated by the value of the auto-coherent diffraction domain size in the range 26–28 nm obtained by the Rietveld analysis. As shown below these values are consistent with HRTEM measurements.

### *3.2. High-field magnetization measurements*

Isothermal magnetization curves $M(H)$ obtained at 4.2 K are reported in figure 3 for $SmFe_{9-y}Ga_yC$ for various Ga contents. It must be emphasized that saturation is not reached, which gives evidence for a magnetocrystalline anisotropy among the highest known in these kinds of systems. The saturation magnetization $M_S$ was deduced using the saturation approach law $M(H) = M_S + a/H^2$.

In the case of $SmFe_{8.75}Ga_{0.25}C$, as an example, we found $\mu_0 M_S = 1.21$ T (15.61 $\mu_B$/f.u.). The average iron moment ($\langle\mu_{Fe}\rangle$) is calculated from the saturated moments, assuming an

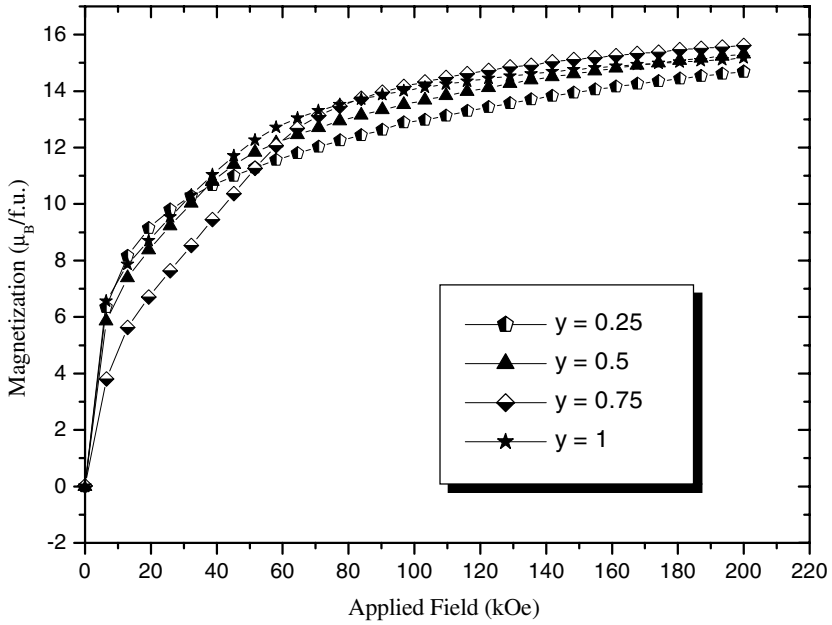


**Figure 3.** Magnetization curve of $SmFe_{9-y}Ga_yC$ (for $y = 0$, 0.25, 0.5, and 1) at 4.2 K.

opposing magnetic moment of each samarium equal to 0.90 $\mu_B$. $\langle\mu_{Fe}\rangle$ was found to increase slightly with Ga content from 1.78 to 2.00 $\mu_B$, respectively, for $y = 0.25$ and 1.

### *3.3. Curie temperature*

Figure 4 reports the Curie temperature evolution versus Ga content for the non-carbonated and carbonated 1/9 $P6/mmm$ alloys and their homologous 2/17 $R\bar{3}m$ compounds. The Curie temperature of the carbonated 1/9 $P6/mmm$ alloys decreases linearly with a slope of 25 °C per Ga atom from 680 K for $y = 0.25$ to 644 K for $y = 1$, remaining always above the Curie temperature of the 2/17 $R\bar{3}m$ carbides ($T_C = 665$ K for $x = 0.5$ to 632 K for $x = 2$).

As shown in figure 4, the Curie temperature values of the 1/9 carbides are higher than those of the non-carbonated 1/9 alloys. This behaviour is due to the magnetovolumic effect induced by carbonation. However, the unit-cell volume expansion is anisotropic as shown by the modifications of the unit-cell parameters and the atomic positions. Table 1 shows the evolution of the interatomic distances as a function of Ga content. It must be outlined that the reduction of the antiferromagnetic $Fe_{2e}$–$Fe_{2e}$ dumbbell distances below the critical value of 2.45 is balanced by the increase of the 3f octahedral site volume relevant to C insertion. The octahedral 3f site with $Fe/Ga_{3g}$ apex reveals the combined C and Ga influences. Under carbonation, the volume increase of the 3f site is 6.33% higher for $SmFe_{8.75}Ga_{0.25}C$ than for the C site of $Sm_2Fe_{16.5}Ga_{0.5}C_2$ while the increase is reduced to 4.44% for $SmFe_8GaC$ compared to that of $Sm_2Fe_{15}Ga_2C_2$. As a function of Ga content, the $T_C$ enhancement under carbonation is gradually reduced by the dilution of the positive $Fe_{3g}$–$Fe_{3g}$ interactions under Ga substitution and the concomitant increase of the negative $Fe_{2e}$–$Fe_{2e}$ dumbbell interaction.

### *3.4. Mössbauer spectrum analysis*

Figure 5 shows the experimental Mössbauer spectra of the $Sm(Fe, Ga)_9C$ series at room temperature. They are complex and magnetically ordered spectra resulting from the

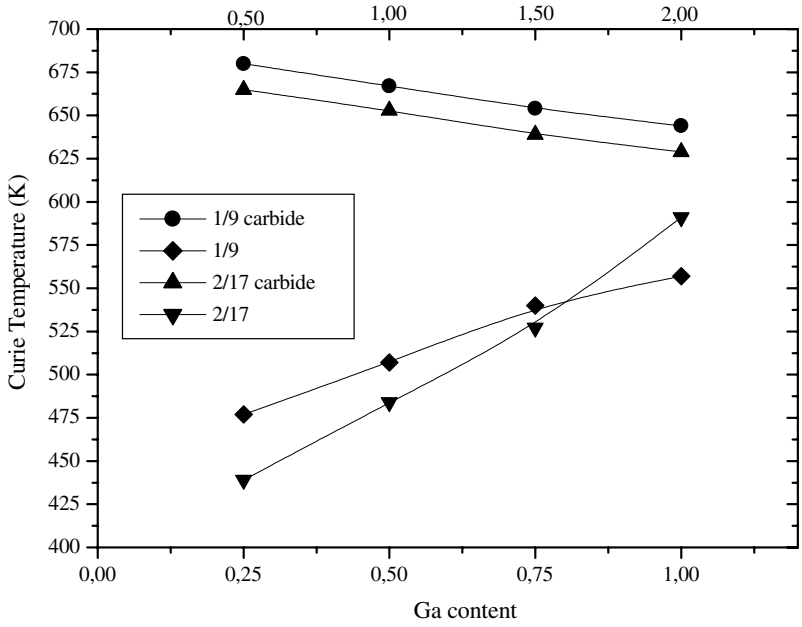


**Figure 4.** Curie temperature versus Ga content for $P6/mmm$ and $R\bar{3}m$ phases and their carbides.

**Table 1.** Interatomic distances for the $P6/mmm$ (a) non-carbonated $SmFe_{9-y}Ga_y$ and (b) carbonated $SmFe_{9-y}Ga_yC$ for $y = 0.25$ and 1.

| | Distance (Å) $y = 0.25$ | | Distance (Å) $y = 1$ | | Number of near | |
|---|---|---|---|---|---|---|
| Site | (a) | (b) | (a) | (b) | neighbours | Notation |
| 6l | 2.47 | 2.48 | 2.50 | 2.49 | 2 | 6l |
| | 2.44 | 2.47 | 2.44 | 2.46 | 4 | 3g |
| | 2.76 | 2.82 | 2.75 | 2.80 | 2 | 3g |
| | 2.75 | 2.77 | 2.77 | 2.77 | 2 | 2e |
| | — | 1.87 | — | 1.87 | 1.33 | 3f |
| | 2.43 | 2.48 | 2.44 | 2.49 | 1 | 1a (Sm) |
| 2e | 2.42 | 2.43 | 2.40 | 2.41 | 1 | 2e |
| | 2.62 | 2.67 | 2.63 | 2.66 | 6 | 3g |
| | 2.75 | 2.77 | 2.77 | 2.77 | 6 | 6l |
| | — | 2.80 | — | 2.78 | 4 | 3f |
| | 2.95 | 2.99 | 2.98 | 2.99 | 1 | 1a (Sm) |
| 3g | 2.44 | 2.47 | 2.44 | 2.46 | 4 | 6l |
| | 2.47 | 2.52 | 2.48 | 2.51 | 4 | 3g |
| | 2.62 | 2.67 | 2.63 | 2.66 | 2 | 2e |
| | — | 2.10 | — | 2.10 | 1.33 | 3f |
| | 3.23 | 3.28 | 3.24 | 3.27 | 2 | 1a (Sm) |

convolution of numerous sub-spectra. The existence of three non-equivalent crystallographic sites, the statistical substitution of gallium for iron in the 3g site, the existence of Fe–Fe dumbbells connected to the Sm vacancies, and the partial occupation of the 3f one by carbon are

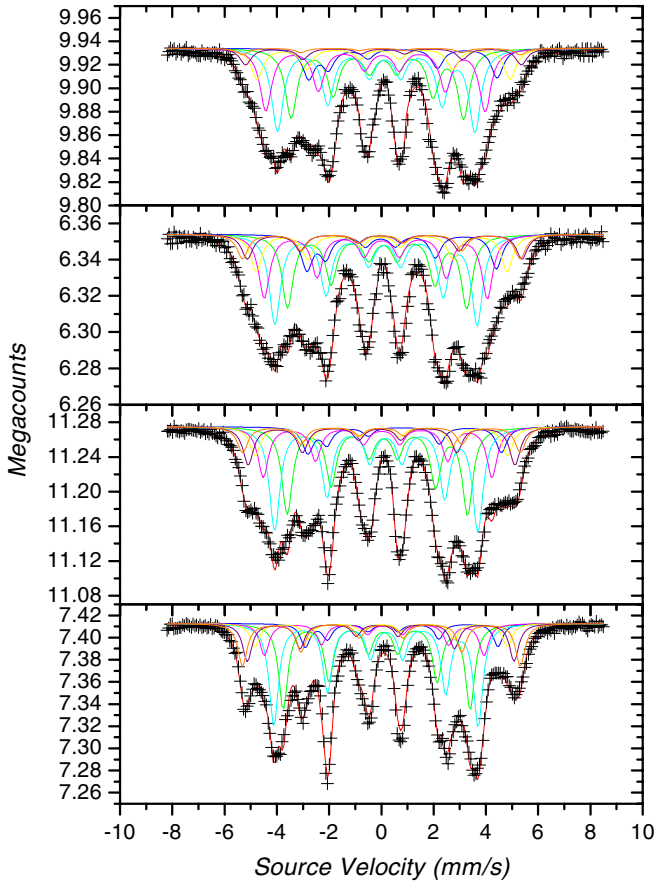


**Figure 5.** The 293 K Mössbauer spectra of $SmFe_{9-y}Ga_yC$ with $y = 0.25, 0.5, 0.75$, and 1.

responsible for such complexity. It must be outlined that for such spectra the use of numerous parameters would lead to a good simulation; however, the right solution is that linked to a pertinent physical model connected to the structure characteristics. The coherency of the derived hyperfine parameters then justifies the validity of the analysis.

For each Ga content, in the first step of the fitting procedure, the abundances of the various iron sites were maintained as fixed parameters according to the multinomial law assumption, while the hyperfine parameters $\delta$, $H$, and $2\epsilon$ were considered as free fitting parameters. It must be emphasized that the number of the sub-sites used for the fit remained physically significant, as the line-width was equal to 0.27 mm $s^{-1}$. The sharpness of line-width, equal to that found in the non-carbonated alloys, attests to the fact that the site number is only affected by Ga substitution and not by carbon insertion, which only rules the values of the hyperfine parameters of each crystallographic site.

In a second step, an average isomer shift value was assigned to each crystallographic family 2e, 3g, and 6l according to the relationship between isomer shift and the WSC sequence 2e $>$ 3g $>$ 6l. In the last step of the fit, all parameters were free.

The Wigner–Seitz cell (WSC) volumes have been calculated (see table 2) for the $P6/mmm$ structure in a way that takes into account the statistical distribution of Ga in 3g sites, the 6l hexagons around the $c$ axis, the Sm vacancies associated to the dumbbells. As a consequence,

**Table 2.** Wigner–Seitz cell derived near-neighbour environments and volumes in $SmFe_{8.5}Ga_{0.5}C$, $P6/mmm$.

| Site | Sm (1a) | Fe (2e) | Fe (6l) | Fe (3g) | Iron near neighbours | WSV $(Å)^3$ |
|---|---|---|---|---|---|---|
| Sm (1a) | 0 | 8 | 4 | 8 | 17 | 34.68 |
| Fe (2e) | 2 | 1 | 6 | 6 | 12.36 | 20.57 |
| Fe (6l) | 1 | 2 | 2 | 6 | 9.36 | 13.60 |
| Fe (3g) | 2 | 2 | 4 | 4 | 9.57 | 14.13 |

we have simulated the partial occupation in an appropriate crystallographic subgroup. The easiest possibilities is given by $P_1$ subgroup with $a = 2a$, $b = 3b$, and $c = c$. The WSC volumes play a major key role in the Mössbauer spectrum analysis as they are directly correlated with the isomer shift as explained below. The WSC volumes have been calculated by means of Dirichlet domains and coordination polyhedra for each crystallographic family. We have used the procedure of radical planes, which results in a space partition without gaps between the polyhedra [8]. The radius values [9] of 1.81, 1.26, and 1.41 Å have been used respectively for Sm, Fe, and Ga.

The compositional dependences of the site isomer shift and hyperfine magnetic field, for the three inequivalent iron sites, are shown, respectively, in figures 6(a) and (b).

The effect of carbonation and Ga substitution can be explained on the basis of either the average isomer shift $\bar{\delta}$ or the individual site isomer shift $\delta$.

The isomer shift is affected by the presence of the interstitial element. From $SmFe_{9-y}Ga_y$ to their carbides we have noticed an increase of the isomer shift at the Fe nuclei. The increase of $\bar{\delta}$ reflects the decrease of electron density with carbon insertion. It indicates a charge transfer from the rare-earth 6s orbital into the carbon atoms combined with the effect of the volume expansion, which is quite significant. Similar trends on the isomer shift are observed [10] upon nitrogen or carbon insertion, meaning that whatever the interstitial element introduced in this crystal structure a modification of the rare-earth 6s orbital is observed. This is not surprising, because the interstitial elements are the first neighbours of the rare earth. Moreover, the short bonds observed between Sm and the interstitials bear witness to a hybridization. In agreement with the Wigner–Seitz cell analysis of three inequivalent iron sites, the sequence of $\delta$ 2e > 3g > 6l follows the sequence of Wigner–Seitz cell volumes as shown in figure 6(a). Upon carbonation, the general increase in isomer shift results from the unit cell expansion, which decreases the s-electron density at the iron nucleus.

This overall expansion of the lattice results in the well known volume effect on the mean average isomer shift. The decrease of the electron density at the iron nucleus produces an increase in the observed average isomer shift $\Delta\bar{\delta}$ of 0.099 mm $s^{-1}$. This value agrees with the increase of 0.1 mm $s^{-1}$ reported by Hu *et al* on $R_2Fe_{17}N_x$ [11], who prefers to estimate the volume effect on the isomer shift by calculating $\Delta\bar{\delta}/\Delta \ln V$. Phenomenologically, the effect of volume change on the isomer shift of iron, in bcc Fe, is well established, $\Delta\bar{\delta}/\Delta(\ln V) = 1.3$ mm $s^{-1}$ [12], and this gives a gauge by which additional influences of chemical bonding may be assessed. Taking the relative volume expansion ($\Delta V/V = \Delta \ln V$) values, we found that $\Delta\bar{\delta}/\Delta \ln V$ on carbonation is 2.07 mm $s^{-1}$. This is larger than that for $R_2Fe_{17}N_x$ ($\Delta\bar{\delta}/\Delta \ln V = 1.7$ mm $s^{-1}$ [11]), which suggests that the interband electron transfer on carbonation in $SmFe_{9-y}Ga_y$ is stronger than in the 2:17 nitrides.

The effect of carbonation on the isomer shift may be discussed on the basis of the individual site isomer shifts. Upon carbonation, the unit cell volume expands, and hence the WSC volume of each site increases. The values of isomer shift for the different iron sites in the carbides are in

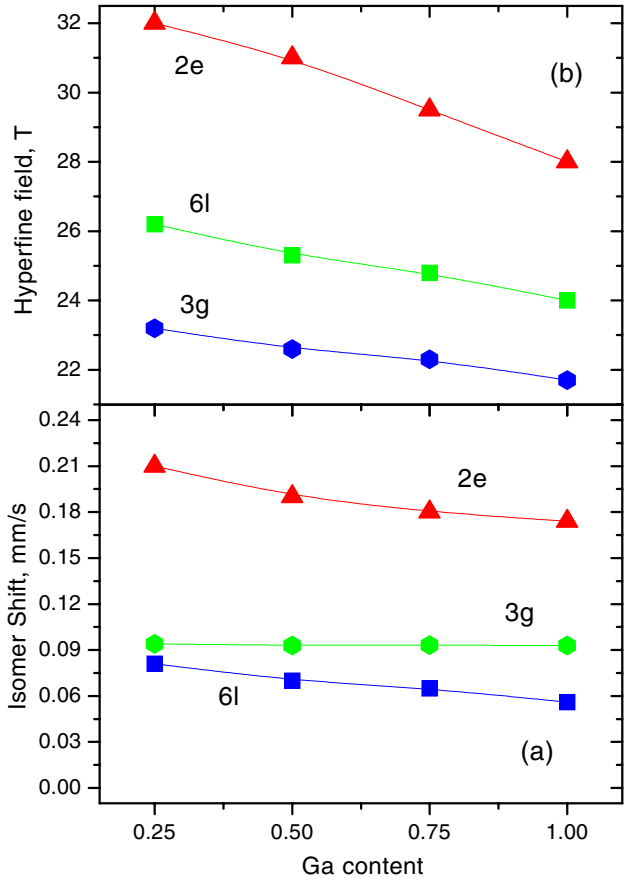


**Figure 6.** The compositional dependences of the isomer shift (a) and hyperfine fields (b) at 293 K for hexagonal $P6/mmm$ $SmFe_{9-y}Ga_yC$ structure. The solid line is a guide for the eyes.

good agreement with those obtained for $SmFe_{9-y}Ga_y$ [2]. In order to understand the effect of carbonation on the isomer shift of an individual iron site, the volume increase upon carbonation and the presence of a near-neighbour carbon atom must be considered.

For $SmFe_{8.75}Ga_{0.25}C$, the distances $Fe_{2e}$–C, $Fe_{3g}$–C, and $Fe_{6l}$–C are respectively equal to 2.78, 2.10, and 1.87 Å, with a number of carbon neighbours respectively equal to 6, 2, and 2. The calculated $\Delta\delta/\Delta(\ln V_{WSC})$ obeys the following sequence: 0.961, 0.685, and 0.458 mm $s^{-1}$ for 2e, 3g, and 6l sites. Therefore, the sequence is ruled by the combined effect of C neighbours and their distance to the corresponding iron species.

From figure 6(a), it appears that $\delta\{2e\}$, $\delta\{6l\}$ decrease slightly with Ga increasing (0.071% and 0.098% per Ga atom for respectively 2e and 6l) while $\delta\{3g\}$ remains quasi-constant within the experimental uncertainty. In the non-carbonated series [2], all isomer shifts were increasing versus $y$ but with a slackening for $\delta\{3g\}$. The specific behaviour of $\delta\{3g\}$ corroborates the location of gallium in this site but, in a first approximation, the key role in the isomer shift values and their evolution is played by carbon.

The mean hyperfine field $\bar{H}$ increases after carbonation; however, this increase is reduced with Ga increasing. As an example, for $y = 0.25$, $\bar{H}$ increases from 23.9 to 27.1 T for the carbonated alloy while for $y = 1$ both values are very close: 24.7 T for the 1/9 alloy; 24.6 T

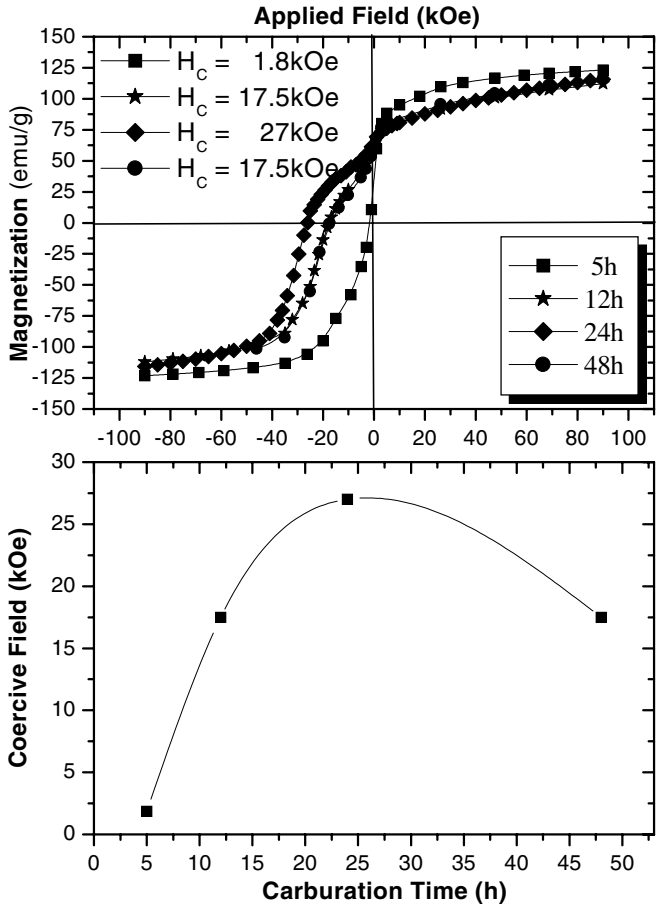


**Figure 7.** Coercive field, at room temperature, versus the carbonation time in $SmFe_{8.75}Ga_{0.25}C$, annealed at 983 K.

for the carbide. The hyperfine field is dominated by the Fermi contact term with two opposite contributions, the positive $H$ 4s conduction electrons and the negative core electron polarization term $H_C$. The competition between these two terms leads to a reduction of the resulting negative hyperfine field that might be explained by a dilution effect correlated to the increasing number of Ga neighbours.

The magnetic hyperfine field evolution is shown as a function of Ga content in figure 6(b) for each non-equivalent crystallographic site. The hyperfine field assignment is deduced from the isomer shift assignment due to the fact that each non-equivalent crystallographic site is characterized by its proper set of hyperfine parameters $\delta$ and $H$. It turns out that $H\{2e\} > H\{6l\} > H\{3g\}$ and all hyperfine fields are decreasing versus $y$.

### *3.5. Coercivity*

To optimize the carbonation process various alloys were prepared versus carbonation duration; the maximum of 27 kOe is obtained for 24 h carbonation (figure 7). This evolution can be correlated with the evolution of the crystallographic structure. Indeed, for rather short carbonation times, the carbonation process is not complete, which leads to a weak $H_C$ value.

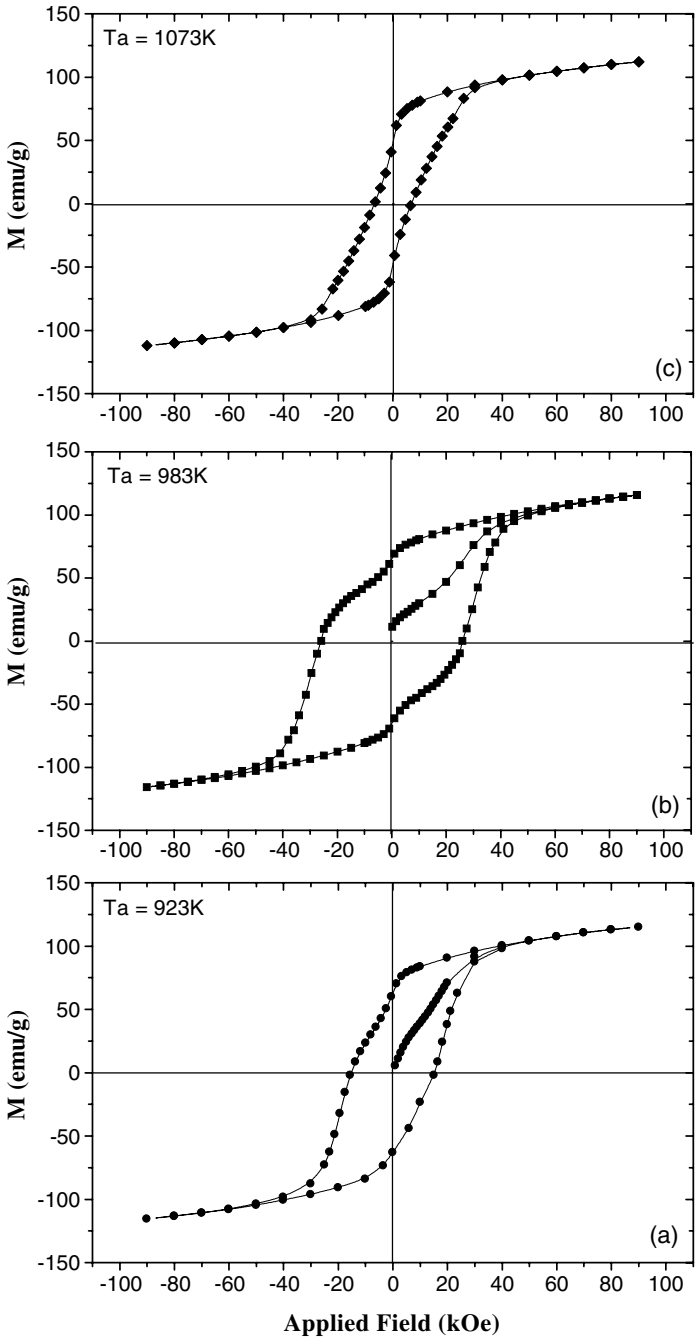


**Figure 8.** Coercive field, at room temperature, in $SmFe_{8.75}Ga_{0.25}C$ for different annealing temperatures: (a) $T_a = 923$ K, (b) $T_a = 983$ K, and (c) $T_a = 1073$ K.

The hysteresis loop of $SmFe_{8.75}Ga_{0.25}C$ measured at room temperature is illustrated in figure 8. The effect of annealing temperature, before carbonation, on magnetic properties is demonstrated. The coercive field increases with increasing annealing temperature up to 27 kOe

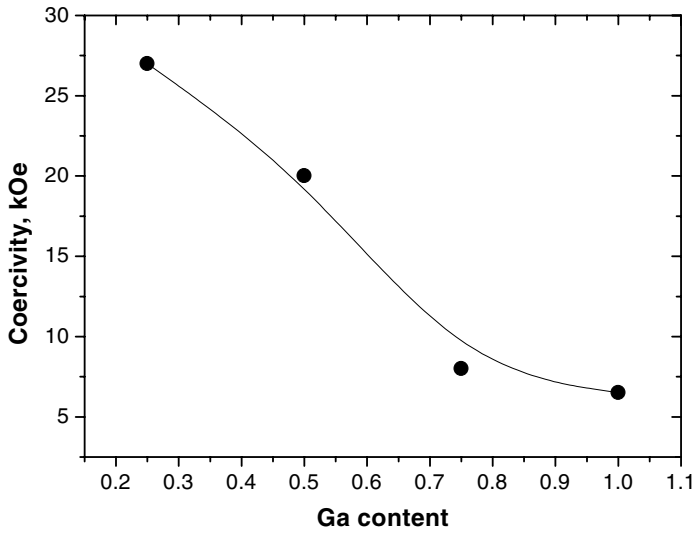


**Figure 9.** Coercive field, at room temperature, versus gallium content in $SmFe_{9-y}Ga_yC$ for indicated $y$ values, annealed at 983 K.

($D = 28$ nm) (figure 8(b)). This value is higher than that obtained in $Sm_2(Fe, Ga)_{17}C_2$ with Cu additive [13] and represents a record in such a kind of materials.

For an annealing temperature of 923 K the coercivity is equal to 18.5 kOe (figure 8(a)). This value might be due to an unfavourable microstructure, probably resulting from a small grain size containing many defects. Furthermore, it is well established that the coercive field $H_C$ decreases with increasing grain size, i.e. with increasing annealing temperature. This is the reason for the reduced $H_C$ value for samples annealed at $T_a = 1073$ K ($H_C = 6.8$ kOe—figure 8(c)).

Figure 9 represents $H_C$ versus gallium content, measured at 90 kOe for $y = 0.25, 0.5, 0.75$ and 1, annealed at 983 K. The $H_C$ values decrease down to 6.8 kOe for $y = 1$. This effect suggests a reduction of the magnetic anisotropy field with increasing Ga content.

HRTEM images confirm the auto-coherent diffraction domain size found by Rietveld analysis. Figure 10 shows an HRTEM image of the $SmFe_{8.75}Ga_{0.25}C$ compound annealed for 30 min at $T_a = 983$ K, with the highest coercivity. According to the HRTEM analysis we observed a size distribution of 20–40 nm. It must be outlined that this grain size distribution originates the non-regular shape of the hysteresis loop (figure 8(b)). The narrowing of this distribution might be obtained by optimizing the milling and the subsequent annealing conditions before carbonation.

Furthermore, the remanence ratio $M_R/M_S$ found around 0.6 is inherent to the nanocrystalline state. $SmFe_{8.75}Ga_{0.25}C$ appears suitable for further permanent magnet applications.

## 4. Conclusions

In this paper, the study of the combined influence of Ga substitution and C insertion in nanocrystalline $P6/mmm$ $SmFe_{9-x}Ga_xC$ alloys ($0 \leqslant x \leqslant 1$) has been carried out for the first time. The carbides have been prepared by a controlled nanocrystallization of high-energy milled powders annealed between 873 and 1200 K, followed by carbonation with heavy hydrocarbon at 693 K. Carbonation induces an anisotropic volume expansion reduced

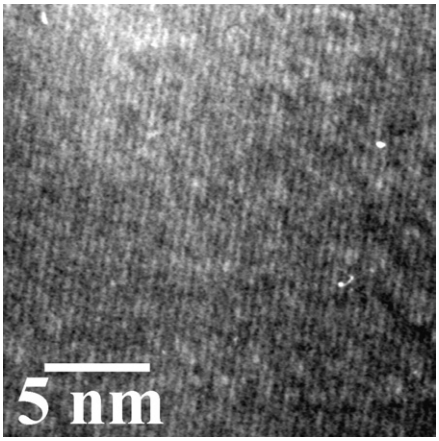


**Figure 10.** High resolution TEM image of $SmFe_{8.75}Ga_{0.25}C$, annealed at $T_a = 983$ K.

with increasing Ga. The increase of the unit cell is 25% higher for $SmFe_{8.75}Ga_{0.25}C$ than for its equilibrium homologous 2/17 alloy, $Sm_2Fe_{16.5}Ga_{0.5}C_2$, and becomes identical to that of $Sm_2Fe_{15}Ga_2C_2$ for $SmFe_8GaC$. The Rietveld analysis corroborates the Ga location in the 3g site.

Magnetization at 4.2 K, up to 200 kOe, gives evidence for a magnetocrystalline anisotropy lying among the highest. The average iron magnetic moment is found to increase slightly with Ga content from 1.78 to 2.00 $\mu_B$ for $x$ equal respectively to 0.25 and 1. The Curie temperatures $T_C$ of the $SmFe_{9-x}Ga_x$ carbides are higher than those of their non-carbonated homologues as expected from the magnetovolumic effect. They remain always 15 K above the Curie temperature of the 2/17 carbides. As a function of Ga content, the $T_C$ augmentation under carbonation is gradually reduced by the dilution of the positive $Fe_{3g}$–$Fe_{3g}$ interactions under Ga substitution and the concomitant increase of the negative $Fe_{2e}$–$Fe_{2e}$ dumbbell interaction.

The good resolution of the Mössbauer spectra makes possible their detailed analysis based on the counting of the various Fe sites, resulting from the binomial distribution of the $Fe_{2e}$ dumbbells linked to the Sm vacancies, the statistical distribution of the Ga atoms in the 3g site and the existence of the 6l hexagons around the $c$ axis. The role of the C insertion is shown by the increase of isomer shift and hyperfine field compared to the corresponding values in the non-carbonated alloys. The isomer shift increase is related to the decrease of the electron density at the Fe nuclei due to the volume expansion and the chemical bonding influences. It reveals a charge transfer from the 6s orbital of the rare-earth atom into the carbon atoms stronger than in 2:17 nitrides. The hyperfine field increase, reduced with Ga content, reflects the enhancement of the negative core electron polarization term of the Fermi contact term, reinforced by the C hybridization. The hyperfine parameter assignment to each individual crystallographic site has been performed according to the relationship between isomer shift and Wigner–Seitz cell volumes, calculated specifically with the use of the $P1$ space group, taking into account the partial occupation of the crystallographic sites. It results in the following sequences: $\delta\{2e\} > \delta\{3g\} > \delta\{6l\}$ and $H\{2e\} > H\{6l\} > H\{3g\}$.

The coercive field $H_C$ of the $SmFe_{9-x}Ga_xC$ alloys is ruled by the annealing temperature of the non-carbonated alloys in relation to grain size. $H_C$ increases up to 27 kOe for $SmFe_{8.75}Ga_{0.25}C$, which represents with $T_C$ equal to 680 K a potential candidate for high-performance magnet applications.

## References


[1] Djéga-Mariadassou C and Bessais L 2000 *J. Magn. Magn. Mater.* **210** 81
[2] Bessais L, Dorolti E and Déga-Mariadassou C 2005 *J. Appl. Phys.* **97** 013902
[3] Bessais L and Djéga-Mariadassou C 2001 *Phys. Rev.* B **63** 54412
[4] Rodríguez-Carvajal J 1993 *Physica* B **192** 55
[5] Pinoche J C, Guillot M and Marchand A 1989 *Physica* B **155** 407
[6] Kirchmayr H R and Burzo E 1990 *Numerical Data and Functional Relationships in Science and Technology* vol 19 *Crystal and Solid State Physics* (Berlin: Spinger) p 250
[7] Villards P and Calvert L D 1991 *Pearson's Handbook of Crystallographic Data for Intermetallic Phases* (Metals Park, OH: ASM International)
[8] Koch E and Fischer W 1996 *Z. Kristallogr.* **211** 251
[9] Teatum E T, Gschneidner K A and Waber J T 1960 *US Department of Commerce Washington DC* LA:2345
[10] Middleton D P, Mulder F M, Thiel R C and Buschow K H J 1995 *J. Magn. Magn. Mater.* **146** 123
[11] Hu B P, Li H S, Song H and Coey J M D 1991 *J. Phys.: Condens. Matter* **3** 3983
[12] Williamson D L, Bukshpan S and Ingalls R 1972 *Phys. Rev.* B **6** 4194
[13] Zhang S Y, Sun Z G, Zhang H W, Han B S, Shen B G, de Boer F R and Buschow K H J 1999 *Appl. Phys. Lett.* **75** 546